Research Article **Open Access**

Simon M. Barrans*, Goodarz Khodabakhshi, and Matthias Muller

Classical and numerical approaches to determining V-section band clamp axial stiffness

Abstract: V-band clamp joints are used in a wide range of applications to connect circular flanges, for ducts, pipes and the turbocharger housing. Previous studies and research on V-bands are either purely empirical or analytical with limited applicability on the variety of V-band design and working conditions. In this paper models of the V-band are developed based on the classical theory of solid mechanics and the finite element method to study the behaviour of the V-bands under axial loading conditions. The good agreement between results from the developed FEA and the classical model support the suitability of the latter to model V-band joints with diameters greater than 110 mm under axial loading. The results from both models suggest that the axial stiffness for this V-band cross section reaches a peak value for V-bands with radius of approximately 150 mm across a wide range of coefficients of friction. Also, it is shown that the coefficient of friction and the wedge angle have a significant effect on the axial stiffness of V-bands.

Keywords: V-band clamp; turbocharger; axial stiffness; finite element analysis

DOI 10.1515/eng-2015-0010
Received August 12, 2014; accepted November 24, 2014

1 Introduction

V-band retainers as shown in Figure 1 are utilised to form a joint between a pair of circular flanges for hoses, pipes, ducts, pipelines, turbocharger housings, and many more applications. Their simple configuration and reliable operation make them a good alternative to traditional clamping devices. V-band retainers were invented during the Second World War by the Marman products company and are presently used in a wide range of applications in the aerospace and automotive industries. When compared to traditional re-assembling joints using bolts and screws offering the same strength, V-band retainers have many benefits. As only one T-bolt nut needs to be tightened they are faster and easier to assemble and re-assemble. Since the flange load is more evenly distributed and the flanges contain fewer stress raisers, they can be manufactured with less material, leading to a much lighter joint. As smaller flange thicknesses and no movement of the fastener in the axial direction are required, V-band joints need less space, which makes them very effective where a compact joint is needed. Especially in automotive and aerospace applications, these latter two benefits are crucial as weight and space reductions will reduce costs. The mechanism by which a V-band retainer creates a joint is easily understood. Placing the retainers around a pair of flanges the T-bolt nut is tightened which results in reducing the circumference and thereby creating a radial force, as can be seen in Figure 2. The wedging action created by the radial force then generates an axial clamping force, pressing both flanges together.

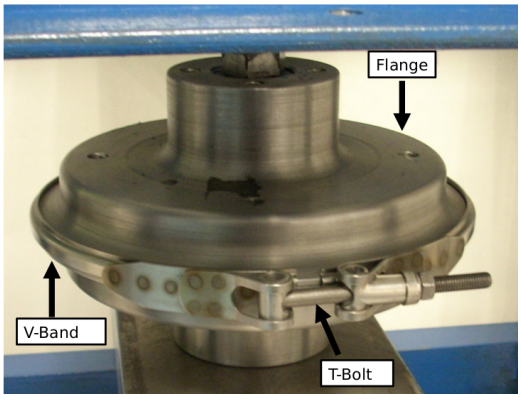

Figure 1: V-band retainer assembled to a pair of test flanges.

The type of Marman clamp that has received the most attention in the literature consists of a number of individual, relatively stiff V-segments held onto relatively flexible flanges with a flat band. In 1966 Wilkey [1] was granted a patent for an experimental rocket system where a key feature was the use of a Marman clamp to hold the final velocity package in place. This method of holding packages such as satellites into delivery vehicles remains the pre-

***Corresponding Author: Simon M. Barrans:** School of Computing and Engineering, University of Huddersfield, Queensgate, Huddersfield, West Yorkshire, HD1 3DH, UK, E-mail: s.m.barrans@hud.ac.uk
Goodarz Khodabakhshi, Matthias Muller: School of Computing and Engineering, University of Huddersfield, UK

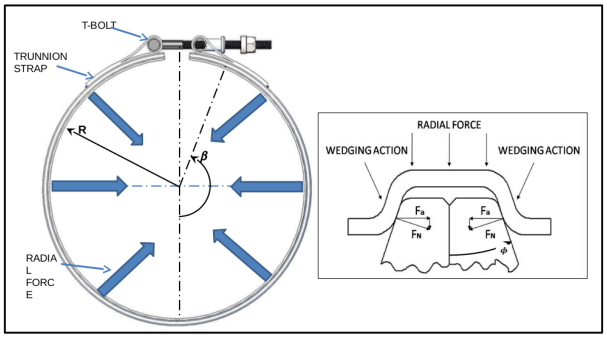

Figure 2: Working principle of V-band clamp assembled to a pair of flanges.

ferred method as described by NASA[1] and Stravrindis *et al.* [2]. Release of the satellite once in the correct orbit is achieved by exploding the T-bolt using a pyrotechnic device. Lazansky [3] reviewed and discussed the design of Marman clamp-band separation systems and highlighted the importance of creating a predictable joint stiffness using these clamps. It was also noted that stiffness under axial tension was more difficult to achieve than compressive stiffness.

As described by Meyer [4], Marman clamps may also be used to hold the various stages of rockets together where again, easy release of the clamp is a significant advantage. Rome *et al.* [5] proposed a 3D finite element model to determine the structural capability of such clamp band systems and investigate the effects of physical parameters such as friction and band pre-tension. Increased pretension in the band and increased coefficient of friction both increased the axial clamping load.

A variation of the Marman style clamp was examined by Barlam and Feldman [6]. They considered a clamp used to connect the stages of missiles sitting inside the cylindrical sections of the missile body. The connection's flanges therefore project radially inwards and the clamp segments have the V profile on their outer radius. Two different commercial finite element software namely, NASTRAN and MARC were employed and both axisymmetric and three dimensional models were analysed. The paper concluded that the MARC code was easier to use for three dimensional models but experimental work was required to verify the results. In addition to the bands discussed above, another type of V-band widely used in the automotive and aerospace industries is formed from a continual, flexible V-section band assembled around relatively stiff flanges. Whilst some of the work undertaken on discrete V-section segment clamps may be transferable to continuous V-section band clamps, there will be significant differences.

This second type of band first appears to have been studied by Mountford [7] who examined their application as a method of connecting together the housings of diesel engine turbochargers. That work was limited as it was based on empirical data with the results of a series of pressure tests being extrapolated out to other load cases. Analytical (Shoghi *et al.* [8]) and a finite element (Shoghi *et al.* [9]) models were developed for the analysis of stresses in V-section band clamps that suggested a variation in working stresses due to uncontrolled operating parameters and manufacturing tolerances associated with this type of band. These results were backed up with experimental data and an updated method of determining the axial load generated by an assembled v-band clamp joint was presented (Shoghi *et al.* [10]).

Recently Barrans *et al.* [11] and Muller [12, 13] presented an axisymmetric finite element model to study failure mechanisms in V-bands under axial loading. They categorized failure of V-band joints under axial loading as taking one of two forms. Firstly, small separation of the flanges with elastic deformation of the V-band retainer, where the flanges reconnect again after the axial load is taken off. Although no physical damage takes place, this failure is undesirable, as especially in turbocharger applications, fluid leakage may occur or components may clash (Shoghi [14]), and in aerospace applications failure of the whole system due to chatter may occur (Stavrindis *et al.* [2]).

Secondly, irrecoverable separation of the flanges, which occurs when the V-band retainer moves over one or both flanges, and hence total failure of the mechanical V-band joint occurs. This would be unacceptable in many applications. For example, as Shoghi *et al.* [10] have observed, such a failure on a turbocharger would lead to a lack of containment of parts with very high kinetic energies. The impact of flange and V-band geometry on the ultimate axial load capacity of v-band joints was studied by Barrans *et al.* [11] and Muller [13].

The previous work described above, on the stiffness of Marman clamp joints has demonstrated that the substantial V-segments in the Marman clamp are much stiffer than the structure surrounding the joint. However, even with these relatively stiff V-segments some deformation of the segments will occur prior to complete flange separation (as shown by Barlam and Feldman [6]). This is consistent with the work of Bickford [15] and Brown and Durbin [16] who observe that, in order to determine the axial stiffness

1 NASA, Marman clamp system design guidelines, Guideline GD-ED-2214, Goddard Space Flight Centre, 2000.

of a bolted joint, the axial stiffness of both the bolt and the flange are required. These latter references introduce the concept of a loading plane to distribute the externally applied load between the bolt (where it increases load) and the flange (where preload is relaxed). A V-band joint is very similar to a bolted joint but the stiffness of the bolt will be replaced by the stiffness of the band. In this paper, as a first step towards understanding this complex V-band joint system, the stiffer flange structure will be assumed to be rigid. This will allow the stiffness of the V-band to be determined.

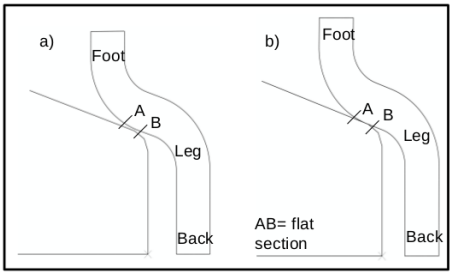

Figure 4: Assembling process of V-band retainer in axisymmetric finite element model, a) un-assembled, b) assembled (T-bolt nut tightened).

2 Finite element analysis of clamp band

The finite element method is employed in this research as a well-established and powerful computational tool in structural mechanics. A three dimensional (3D) finite element model consisting of half the V-band and one flange has been constructed as shown in Figure 3.

An axial displacement constraint was applied to the V-band to enforce the symmetry condition. The V-band was modelled as solid body, applying linear elements with reduced integration as suggested by Dassault Systems[2] and as recommended by Konter [17] for similar cases of contact analyses. Although Konter [17] suggests using a penalty contact algorithm for easier convergence, a Lagrange multiplier contact algorithm was used here to ensure that friction effects were correctly simulated (as recommended by Feng and Prinja [18]). The flange was defined as an analytical rigid body to reduce the complexity of the analysis. Displacements and rotations of the reference point (RP) were constrained to keep the flange in position. It should be emphasised here that since the flange is being modelled as a rigid body, no deformation will take place until the initial preload generated by the V-band is overcome (*i.e.* up to this point the stiffness will appear to be infinite). Only after this point where the flange has separated from its partner will additional load be applied to the V-band. As previous work by Bickford [15] and others has demonstrated, the stiffness at this point (*i.e.* the V-band stiffness) is an important component of the overall joint stiffness.

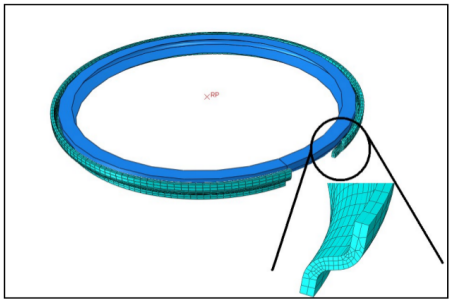

Figure 3: Three dimension finite element model of V-band and flange.

Physically, the V-band retainer is assembled onto a pair of flanges by tightening the T-bolt nut. A tensile circumferential force has been applied to the ends of the V-band to replicate this effect.

This part of the simulation can be seen in Figure 4 (cross section of the 3D model), where in a) a retainer is loosely placed around the flange in the initial position, and b) the retainer is fully assembled and contact established. Although the principal aim of this research was to determine the initial stiffness of the V-band in the joint, it was necessary to utilise a large sliding contact formulation due to the large relative movement of the V-band during this initial tightening stage. It should also be noted that whilst in an ideal V-band joint the contact point will be on the flat section of the wedge, as shown in Figure 4(b), the contact region in these models was extended to include both fillet radii on the inner surface of the V-section.

Tightening the T-bolt generates an axial clamping load (or preload) pushing both flanges together. This was reported in the first step of the finite element analysis as an axial reaction force at the flange's reference point (RP). In the second stage of the analysis an axial displacement was applied to this reference point. The reaction force generated then represented an axial force applied to the joint. The axial stiffness of the V-band was calculated as the rate of change of reaction force with respect to applied displacement at the reference point. This rate was found at a displacement of 0.002 mm to represent an initial stiffness. It should be noted that as predicted, up to the point where

2 Dassault-Systems, Getting Started with ABAQUS v6.7 Section 4 Using Continuum Elements, 2007b.

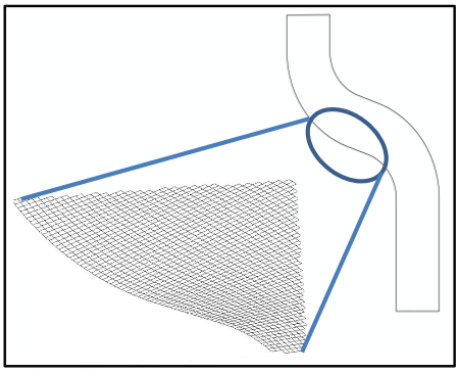

Figure 5: Axisymmetric model mesh density.

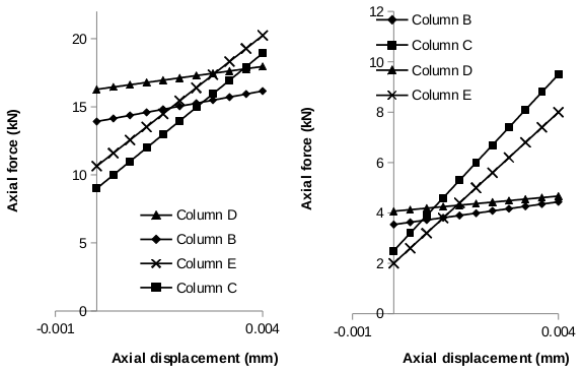

Figure 6: Force- displacement results from 3D and axisymmetric models with coefficient of friction 0 and 0.3: (a) small band (radius=157 mm) (b) large band (radius=557 mm).

the axial clamping load is exceeded, there is no displacement of the reference point and the stiffness of the assembly is infinite.

Due to model size limitations the 3D model described employs a relatively coarse mesh. On the V-band the contact state is determined at the slave nodes. As the analysis progresses, the contact point can move across the contact surface and switches from one node to another. Since there are only six nodes across the contact surface, this switch represents a significant portion of the possible contact area. Hence, a source of inaccuracy has been introduced.

To allow a much finer mesh to be used in the contact area without increasing computational cost, an axisymmetric model of the type investigated by Barlam and Feldman [6] and Rome *et al.* [5] was generated. The boundary conditions for the axisymmetric model are similar to the 3D model except that as in the previous work, tightening of the V-band is simulated as a negative thermal strain to shrink it onto the flange. The T-bolt load is calculated by integrating the resultant circumferential force over the V-band cross section. Manual iteration was required to determine the temperature change required to generate the desired T-bolt load. The disadvantage of the axisymmetric model is that the non-uniform contact pressure around the circumference reported by Shoghi [14] cannot be simulated. In order to simulate the very small contact region between the V-band and the flanges, a high mesh density was used with 41 elements through the thickness of the band and 320 along the length of the profile, as shown in Figure 5.

To compare the 3D and axisymmetric modelling approaches, analyses were carried out on 157 mm and 557 mm radius bands with coefficients of friction of 0 and 0.3. The results are shown in Figure 6. Similarity in stiffness (*i.e.* gradient of the graphs) from 3D and axisymmetric models suggest the suitability of the axisymmetric model as the alternative to 3D model with the benefits of reduction in computational cost and minimisation of the potential error due to a coarse mesh. Therefore, the axisymmetric model is employed in the rest of the paper for finite element modelling.

3 Theoretical prediction of axial stiffness

In addition to the finite element model, a model was developed based on classical solid mechanics theory to study the behaviour of V-bands under axial loading. For the purpose of this analysis and to reduce the complexity of the problem, it is assumed that initial contact between the flange and V-band is located on the flat section of the V-band, remains on the flat section during the axial displacement and the section angle has not been altered by applying an excessive T-bolt load. It will also be assumed that during initial deformation of the band, stiffness will be linear. This is a reasonable restriction of the model as this initial stiffness will be of greatest interest in most applications.

Two forms of deformation are considered: circumferential expansion of the band with no deformation of the cross section and section deformation with no circumferential deformation. The two theories are then combined.

3.1 Ring theory (circumferential extension only)

As a result of tightening the T-bolt and movement of the flanges in the axial direction, normal force per unit length,

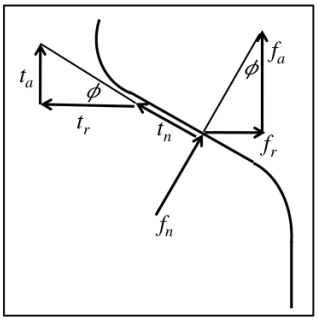

Figure 7: Forces acting on the V-band retainer.

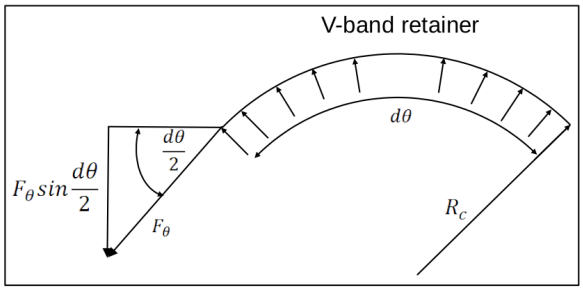

Figure 8: Internal and external forces acting on the V-band retainer.

f_n, is generated and as well as a tangential friction force, t_n, due to the frictional resistance against movement of flanges (in the axial direction). These force components are shown in Figure 7.

The total external load which results in displacement of the flange to band contact point in the axial direction is defined as F_A, and distributed along the inside circumference of the V-band as the axial component, f_a, of the normal force per unit length and the axial component, t_a, of the friction force per unit length. The relationship between these three forces can be expressed in Equation (1)

$$F_A = 2R_c\beta(f_a + t_a), \tag{1}$$

where R_c is the radius at which contact is established between flange and band, where f_a and t_a are acting, and where β is the subtended angle of half the band (see Figure 2). As shown in Figure 7, the relation between f_a and t_a is defined by the following equation:

$$t_a = \mu f_a \tan\phi, \tag{2}$$

where μ is the coefficient of friction.

Combining Equation (1) and Equation (2) gives:

$$F_A = 2R_c\beta f_a(1 + \mu\tan\phi). \tag{3}$$

Considering a segment of the V-band retainer (Figure 8) with an infinitesimal angle, $d\theta$, this externally generated radial force, $f_r - t_r$ creates a reaction force, F_θ, within the V-band acting on both ends of the segment in the circumferential direction.

Using the radius of the contact point between band and flange, R_c, and equilibrium of this segment, the relationship between these two forces is found to be:

$$2F_\theta(\sin(d\theta/2)) = (f_r - t_r)R_c d\theta,$$

$$\text{or, as } d\theta, \text{ tends to zero: } F_\theta = (f_r - t_r)R_c. \tag{4}$$

It is now assumed that the stress in the circumferential direction, σ_θ is uniform over the V-band cross section area, A_B, and will generate a strain in the circumferential direction, ϵ_θ. There will therefore be a change δ_β in the half angle, β, (see Figure 2) of the ring and hence an expansion, δ_r, of the cross section radius, R_s, given by:

$$\epsilon_\theta = (\delta_\beta/\beta) = (\delta_r/R_s) = (F_\theta/EA_B),$$

$$\text{or: } F_\theta = (EA_B\delta_r/R_s). \tag{5}$$

For the geometry of section being considered here the radius of the contact point will be very close to the radius of the section centroid. Hence, it can be assumed that : $R_s = R_c$.

Combining Equations (4) and (5) leads to the following relation:

$$(EA_B\delta_r)/R_c = (f_r t_r)R_c. \tag{6}$$

Considering the relation between f_r, t_r and f_a with reference to Figure 7 ($t_r = \mu f_a, f_r = f_a\tan\phi$) Equation (6) can be written:

$$f_a = (EA_B\delta_r)/(R_c^2(\tan\phi - \mu)). \tag{7}$$

Substituting into Equation (3) then gives the following relationship between applied axial force and ring expansion:

$$F_A = (2\beta EA_B\delta_{ar}(1 + \mu\tan\phi))/(R_c(\tan\phi - \mu)). \tag{8}$$

In order to calculate the axial stiffness of the V-band, the relationship between the total axial force, F_A, and the axial displacement of the contact point, δ_{ar}, is required. Considering the geometry of the band to flange interface:

$$\delta_{ar} = \delta_r\tan\phi.$$

Hence,

$$F_A = (2\beta EA_B\delta_{ar}(1 + \mu\tan\phi))/(R_c\tan\phi(\tan\phi - \mu)). \tag{9}$$

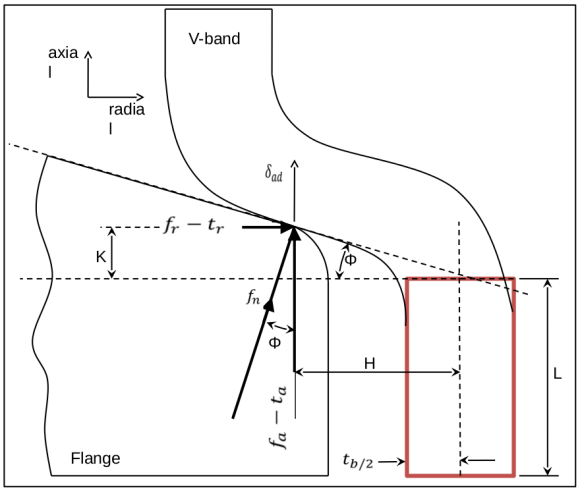

Figure 9: V-band cross section with cantilever (dash line rectangle) assumed in the back.

And the axial stiffness due to ring expansion, k_{ar}, is given as:

$$k_{ar} = (F_A/\delta_{ar}) = (2\beta EA_B(1+\mu\tan\phi))/(R_c\tan\phi(\tan\phi-\mu)). \quad (10)$$

In frictionless case, $\mu = 0$, this degenerates to:

$$k_{ar} = (2\beta EA_B)/(R_c\tan^2\phi). \quad (11)$$

3.2 Development of Section deformation Theory

Whilst the theory presented in the previous section will be applicable to bands where the cross section does not change significantly during loading, where the cross section does change, the theory requires extension, as presented here:

It is assumed that the most significant deformation of the band cross section during axial loading is bending of the back. This is supported by observation of both experimental tests and finite element models. This part of the cross section is assumed to be a rectangular cross section cantilever as shown in Figure 9 (dashed line rectangle), with length L, depth t_b (equal to the V-band thickness), elastic modulus E, and second moment of area I. The foot and leg of the V-band are only considered to calculate K and H which represent the levers for the radial $(f_r - t_r)$ and axial $(f_a + t_a)$ forces respectively.

A suitable method of calculating the cantilever deflection is the unit-load method as presented by Gere and Timoshenko [19] which can be expressed as:

$$\Delta = \int (M_L M_U/EI)dx, \quad (12)$$

where Δ represents a deformation, M_L the moment due to the actual loads, and M_U the moment due to a fictitious unit load applied at the point where the deformation is to be found. Using the unit-load method on a small segment angle $d\theta$, to determine the axial displacement of the contact point, δ_{ad} due to deformation gives:

$$\delta_{ad} = \int (M_L M_U/EI)dx \quad (13)$$
(the integral domain is between 0 and L),

where $M_L = (f_r t_r)(K + x) + (f_a + t_a)H$ and $M_U = H$.
Using the previously developed relationships between the force components:

$$\delta_{ar} = (f_a H/EI)\int\{(\tan\phi - \mu)(K + x) + (1 + \mu\tan\phi)H\}dx,$$
$$\delta_{ad} = (f_a HL/EI)\{(\tan\phi - \mu)(K + 0.5L) + (1 + \mu\tan\phi)H\}. \quad (14)$$

For the small segment with arc length $R_c d\theta$, the second moment of area may be defined as:

$$I = (R_c t_b^3/12)d\theta. \quad (15)$$

Substituting into Equation (11) gives the axial force per unit length as:

$$f_a = \frac{ER_c t_b^3\delta_{ad}}{12HL((\tan\phi - \mu)(K + 0.5L) + (1 + \mu\tan\phi)H)}d\theta. \quad (16)$$

The total axial force, F_A, can be found by integrating around the band:

$$F_A = \frac{ER_c t_b^3\beta\delta_{ad}}{6HL((\tan\phi - \mu)(K + 0.5L) + (1 + \mu\tan\phi)H)}. \quad (17)$$

And the axial stiffness due to section deformation, k_{ad}, is given as:

$$k_{ad} = (F_A/\delta_{ad}) = \frac{ER_c t_b^3\beta}{6HL((\tan\phi - \mu)(K + 0.5L) + (1 + \mu\tan\phi)H)}. \quad (18)$$

3.3 Total joint axial stiffness

The total axial stiffness, k_a, of the band can be defined in terms of the total displacement, δ_a, of the contact point in the joint as:

$$k_a = (F_A/\delta_a) = (F_A/(\delta_{ar} + \delta_{ad})).$$

Or, in terms of the two theories presented above:

$$(1/k_a) = (1/k_{ar}) + (1/k_{ad}). \quad (19)$$

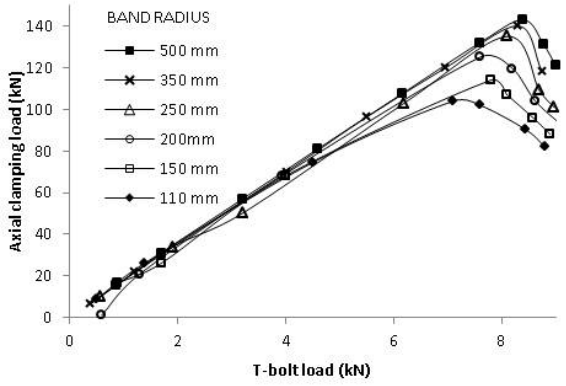

Figure 10: Axial clamping load against T-bolt load (variable V-band radius).

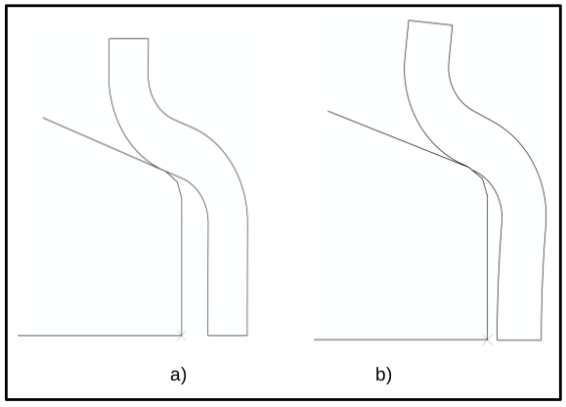

Figure 11: V-band- flange assembly (a) no deflection in v-band and constant contact angle (b) Deformation in v-band and variable (increase) in contact angle.

4 Results and discussion

As described in previous sections, a theoretical and an axisymmetric finite element model have been developed to study the behaviour of V-band joints in the axial direction. In the present study, the geometrical and material data for V-band and flange are listed in Table 1.

4.1 Axial clamping load

As described in section 2, the first step in modelling is to establish initial contact between the V-band and flanges. This simulates tightening the T-bolt and generates an axial clamping load. Figure 10 shows a consistent gradual increase in this axial load as T-bolt load is increased. Also, for low and medium T-bolt loads (less than 7 kN), the resultant axial clamping load is similar for different band sizes. This agrees with the theory presented by Shoghi *et al.* [10] that suggests the initial axial clamping load is independent of the band size. However for high T-bolt loads, a turning point is detected. To investigate this phenomenon, the geometry of the joint system was monitored during application of the T-bolt load. As is shown in Figure 11a, the V-band cross section geometry does not change significantly during the application of lower T-bolt loads and the change in contact angle is very small. However, as shown in Figure 11b, for high T-bolt loads, the V-band starts to deflect during the application of the T-bolt load and the contact angle increases.

An additional observation from Figure 10 is that the limiting T-bolt load at which the assumption of a linear relationship between axial clamping load and T-bolt load becomes unreasonable, occurs at lower T-bolt loads for smaller band diameters. This phenomenon can be understood by considering the two forms of deformation identified in the theory. Ring deformation does not alter the band cross section and therefore does not alter the relationship between axial clamping load and T-bolt load. Large diameter bands have greater ring compliance because there is a greater length of material to expand in the circumferential direction. In fact, for large diameter bands, ring compliance is much higher than section compliance and a substantial T-bolt load has to be applied before significant section deformation takes place. As the band diameter reduces, the ring stiffness increases and becomes comparable to the section stiffness. The transfer of load to section deformation therefore takes place at lower T-bolt loads.

4.2 Axial stiffness

As stated in previous sections, to determine initial axial stiffness of the V-band in the joint (for the finite element model), the flanges were displaced (moved) slightly in the axial direction and the generated axial reaction force at the reference point was recorded. The axial stiffness is then the gradient of such graphs.

Figure 12 shows the stiffness variation with respect to changing V-band radius and T-bolt load with no friction. These results show that the axial stiffness of smaller bands is generally higher than for larger ones, when applying similar T-bolt load. Also, for each band size, the stiffness shows no significant change when increasing the T-bolt load until it drops at high T-bolt loads. This drop off in stiffness is due to the change in contact angle induced by the high T-bolt loads (as explained in the previous section).

The results from the developed theory based on the classical solid mechanics (ring expansion and section de-

Table 1: Data used in the analyses

V-band half section angle (°)	20 degrees
V-band bending radius (r_b)	1.3 mm
Flange contact radius (r_c)	0.8 mm
Elastic modulus (E)	227 kN/mm^2
V-band cross section area (A_B)	13 mm^2
Subtended angle of half the band (β)	180 degrees*
V-band thickness (t_b)	1.3 mm
Lever of axial force F_A (H)	2.16 mm
Lever of radial force F_R (K)	0.786 mm
Length of assumed cantilever for V-band section in combined theory (L)	3.79 mm

* Note: The actual value for β is 167°. This is taken as 180° in the theoretical model to be in line with FEA model for direct comparison.

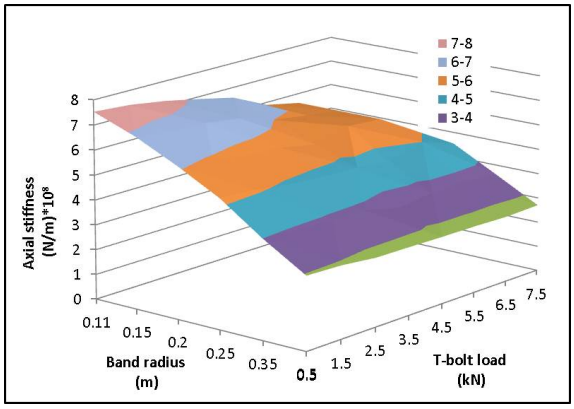

Figure 12: Stiffness as function V-band radius and T-bolt load (no friction, FEA).

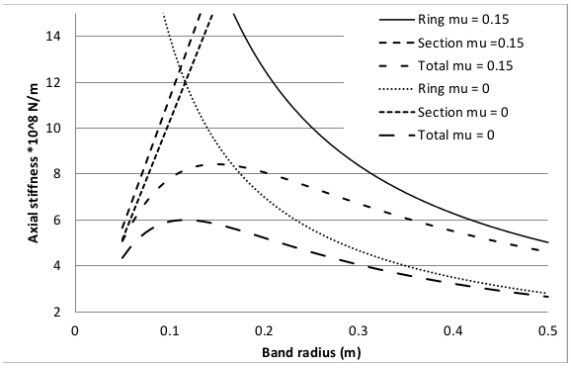

Figure 13: Axial stiffness based on ring expansion and combined theories with friction coefficients of 0 and 0.15.

formation theories) are plotted in Figure 13, for different band sizes also considering the effect of friction (friction coefficient=0.15).

In Figure 13, the section deformation theory shows a rapid linear increase in the axial stiffness with increasing band size. This is to be expected since the cantilever used to approximate the band in this theory has a width equal to the circumferential length of the band. The ring theory predicts that axial stiffness will be inversely proportional to band diameter. Combining the two theories predicts a band diameter where stiffness reaches a maximum. The band diameter giving this maximum stiffness is dependent on the coefficient of friction. It can also be seen that including friction increases axial stiffness.

To further investigate the effect of friction in more detail, the theory was used to calculate the axial stiffness over a range of V-band sizes with variable coefficient of friction. The results shown in Figure 14 confirm that the V-band diameter giving the highest stiffness is indeed dependent on the coefficient of friction. It can also be seen that stiffness increases as the coefficient of friction is increased over the full range of band sizes.

Results from the theory and the finite element models are compared in Figures 15 and 16. Figure 15 shows the axial stiffness values for a range of different band sizes using theory and finite element models with T-bolt loads of 0.5 kN and 6 kN for coefficients of friction of 0 and 0.15. Also, results from the theory and finite element models are compared in Figure 16 for a range of different coefficients of friction for the small (R_c = 110 mm) and large (R_c = 500 mm) band sizes.

Good agreement between the finite element models and theoretical results justifies the utilisation of the proposed theoretical model over this range of band sizes and coefficients of friction. However, it should be noted that at lower V-band diameters, the theoretical model appears to underestimate the stiffness. Two factors may contribute to this: The length of the back, L, is estimated as shown in

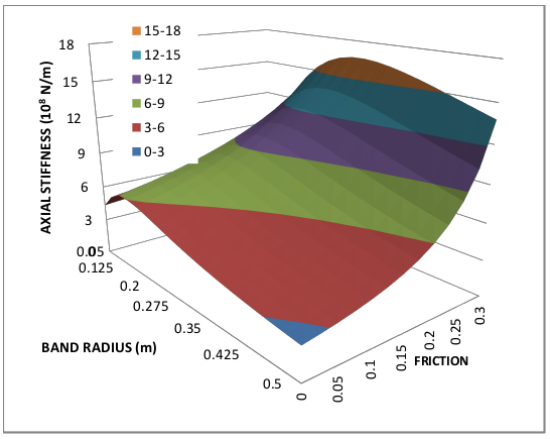

Figure 14: Axial stiffness for different v-band sizes with a range of coefficient of friction from 0 to 0.3 (theory).

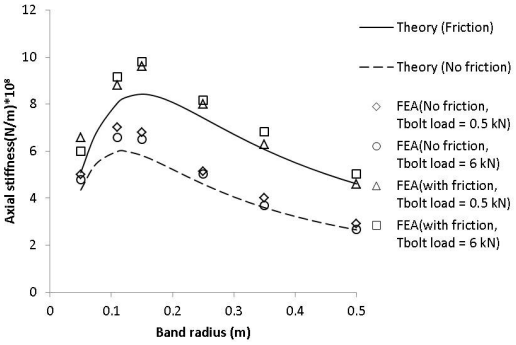

Figure 15: Axial stiffness for different band sizes (theory and FEA, T-bolt load =0.5 kN and 6 kN) with friction (μ =0.15) and without friction.

Figure 9. Reducing L will increase stiffness. Also, as angle ϕ increases due to loading the circumference of the foot of the band must increase. This will increase the resistance to deformation.

The effect of V-band angle, ϕ, on the axial stiffness has also been studied. For the type of V-band used in the present study, this value is equal to 20 degrees. However, this value may change under working conditions (e.g. over tightening of V-band through application of high T-bolt loads). The manufacturer may also wish to change this angle for particular applications.

To ensure that changes to the FEA model were replicated in the theoretical model, the method used to change the band angle was carefully defined. With reference to Figure 17, point b on the flat section of the band was fixed relative to points d and e. The angle change was then defined as a rotation of the flat section of the band around this point. The position of the contact point between the band and the flanges was maintained at point c, the other

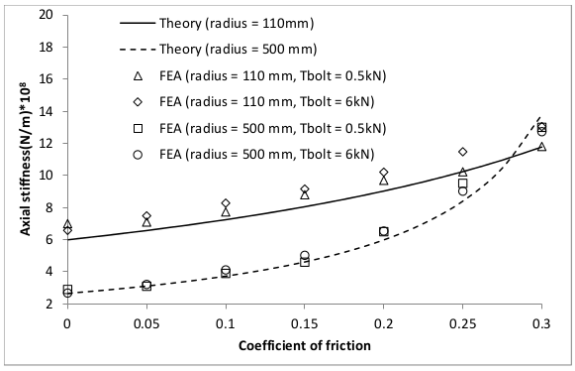

Figure 16: Axial stiffness for different coefficient of friction (theory and finite element model, T-bolt load =0.5 kN and 6 kN).

end of the flat section. In the theoretical model (section 2), the values of H, K and L needed to be adjusted for each angle as these values are dependent on the V-band angle (ϕ). As shown schematically in Figure 17, by changing the angle from ϕ to $\phi + \delta\phi$, the values of H, K and L will change into H', K' and L'. The relations between these parameters are as follows:

$$H - H' = bc(\cos\phi - \cos(\phi + \delta\phi)), \tag{20}$$

$$L' - L = H''(\tan(\phi + \delta\phi) - \tan\phi), \tag{21}$$

$$K = H\tan\phi, \tag{22}$$

$$K' = H'\tan(\phi + \delta\phi), \tag{23}$$

where "bc" ($bc = bc'$) is the length of flat section in the V-band (bc = 0.66 mm) and $\delta\phi$ is change in the wedge angle (ϕ).

The results from the theoretical model of this change in angle study are shown in Figure 18. These suggest that axial stiffness decreases as V-band angle is increased. Figure 19, shows the effect of wedge angle on axial stiffness using both theoretical and finite element models (T-bolt load =6 kN, coefficient of friction=0). This is done for band radii of 110 and 500 mm. The results show a good agreement between the two models. As suggested by both finite element and theory results (Figure 19), for small (radius =110 mm) and large bands (radius = 500 mm), increasing the wedge angle results in the axial stiffness decreasing.

5 Conclusion

A finite element modelling methodology for flexible V-bands on relatively stiff flanges has been produced. This

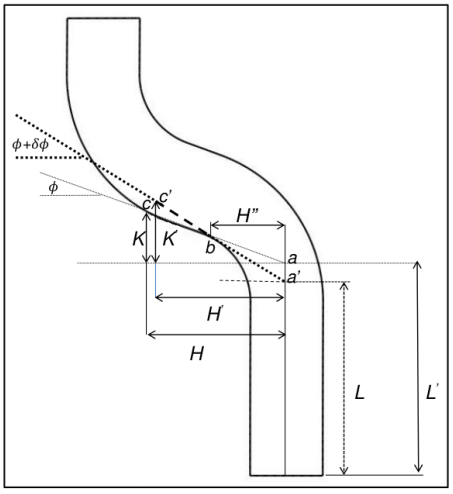

Figure 17: Effect of changing V-band angle on the parameters (H, K and L) used in the theory.

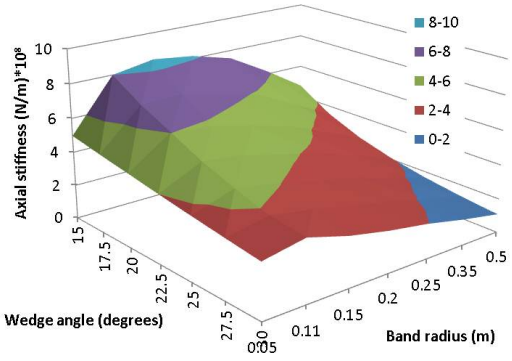

Figure 18: Axial stiffness for different band size and a range of wedge angle (theoretical model).

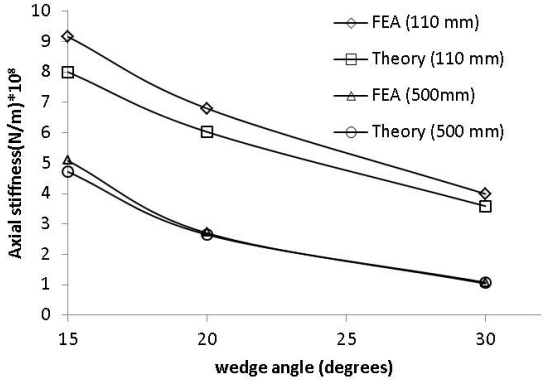

Figure 19: Axial stiffness for a range of wedge angles using both theory and finite element (T-bolt load =6 kN) models.

methodology has generated results that are consistent with previously published results.

The finite element models have demonstrated that, provided that ring stiffness dominates the response of the V-band, axial preload in the joint is independent of band diameter. However, a transfer of load to section deformation will place a limit on axial pre-load that can be generated as T-bolt tension is increased. This limit is lower for smaller diameter bands.

The finite element model also demonstrated that provided band response is dominated by ring stiffness, axial stiffness is independent of T-bolt tension. A classical theoretical model for the axial stiffness of the V-band in the joint has been generated which shows good agreement with the finite element model for band diameters greater than 110 mm and the ranges friction coefficient and wedge angle seen in practice. This theoretical model can therefore be used with confidence to further investigate the factors effecting joint axial stiffness.

Axial stiffness of assembled V-bands is dependent on band diameter. For the band cross section investigated, the peak axial stiffness occurs at band radius of 100 to 200 mm. This peak occurs for larger diameter bands as the coefficient of friction is increased.

6 Further work

It has been demonstrated here that the axial stiffness of assembled V-bands is strongly influenced by the ring stiffness of the band. This ring is broken at the T-bolt to incorporate an assembly including the T-bolt, trunnions and trunnion straps. These components and the interaction between them will impact on band's ring stiffness. Further finite element and experimental work is required to investigate this.

The work carried out here has assumed that the flange is correctly making contact with the band on the flat portion of the band leg. On the common band geometry investigated here, this flat section is small. It has also been shown that increasing the angle of the band (a consequence of contacting on the radii of the leg) will dramatically reduce the axial clamping load and axial stiffness. The impact of manufacturing tolerances on the size of this flat section and the consequences of contacting off this section should be investigated using both finite element models and experimental methods.

The finite element models presented here have been developed for a particular band cross section geometry. These models need to be developed further to incorporate

a range of geometries and the applicability of the classical theory reviewed. The analysis carried out here has allowed the axial stiffness of the V-band to be determined. However, the overall stiffness of the V-band joint will also be influenced by stiffness of the flanges and the position and movement of contact points between the flanges as the joint is deformed. This combined effect will require further analysis.

Nomenclature

A_B = Band cross sectional area
F_A = Applied axial force
F_θ = Internal circumferential force within the band at angle θ
E = Elastic modulus
I = Second moment of area
K = Radial force lever
H = Axial force lever
L = Length of cantilever
M_L = Moment due to the actual loads
M_U = Moment due to unit load
R_c = Radius of flange to band contact point
R_c = Radius of band section centroid

bc = Length of flat section
f_A = Axial component of normal force per unit length
f_r = Radial component of normal force per unit length
k_{ar} = Axial stiffness due to ring expansion
k_{ad} = Axial stiffness due to section deformation
k_r = Total axial stiffness

t_A = Axial component of friction force per unit length
t_b = Band thickness
t_r = Radial component of friction force per unit length
x = Distance along cantilever

Δ = Deformation

ϕ = Subtended half angle of the band
δ_a = Axial displacement
δ_{ar} = Axial displacement of the contact point due to ring expansion
δ_{ad} = Axial displacement of the contact point due to deformation
δ_β = Change in subtended half angle of the band
δ_r = Change in radius Rc
ϵ_θ = Circumferential strain
μ = Coefficient of friction
ϕ = Subtended half angle of the band cross section
θ = Angle around band
σ_θ = Circumferential stress

References

[1] Wilkey J.W., Velocity Package 1966, United States of America, PATENT No. US3260204 A
[2] Stavrinidis C., Klein M., Brunner O., Newerla A., Technical and programmatic constraint in dynamic verification of satellite mechanical systems, Acta Astronaut., 1996, 38(1), 25–31.
[3] Lazansky C., Refinement of a Low-Shock Separation System, Proc. of the 41st Aerospace Mechanisms Symposium, JPL, Pasadena, CA, 2012, 329–343.
[4] Meyer R.X., Elements of Space Technology, San Diego, Academic Press, 1999, 104.
[5] Rome J.I, Goyal V.K., Martino N.E., Techniques for finite element analysis of clamp band systems. In: 50th AIAA/ASME/ASCE/AHS/ASC Structures, Structural Dynamics and Materials Conference, Palm Springs, California, 4–7 May 2009, Reston, VA, American Institute of Aeronautics and Astronautics, 2009.
[6] Barlam D., Feldman E., Solution of contact problems in missile stage connections: NASTRAN versus MARC, In Neittaanmäki P., Rossi T., Majava K., Pironneau O. (Eds), Proc. of the 4th European Congress on Computational Methods in Applied Sciences and Engineering, Jyväskylä, Finland, 24–28 July 2004, Vol. I, Jyväskylä, University of Jyväskylä, 2004, pp.1–15.
[7] Mountford R., Design of clamp joints, Engineering Designers, 1980, 6, 37–40.
[8] Shoghi K., Barrans S.M., Rao H.V., Stress in V-section band clamps, C. J. Mech. Eng. Sci., 2004, 218, 251–261.
[9] Shoghi K., Barrans S.M., Rao H.V., Classical and finite element analysis of V-band retainers, NAFEMS World Congress (Orlando) Florida, 2003.
[10] Shoghi K., Barrans S.M., Ramasamy P., Axial load capacity of V-section band clamp joints, In Proceedings of 8th International Conference on Turbochargers and Turbocharging, pp 273–285, London, 2006.
[11] Barrans S., Muller M., Finite element prediction of the ultimate axial load capacity of V-section band clamps, JPCS, 2009, 181, 1–8.
[12] Muller M., Barrans S., Ultimate axial load capacity of v-band clamp joints, In: Proceedings of Computing and Engineering Annual Researchers' Conference 2009: CEARC'09, University of Huddersfield, Huddersfield, 2009, 14–18.
[13] Muller M., Predicting the ultimate axial load capacity of the joints formed by using V-section band retainers, PhD Thesis, University of Huddersfield, UK, 2011.
[14] Shoghi K., Stress and Strain Analysis of flat and V-section band clamps, PhD Thesis, University of Huddersfield, UK, 2003.
[15] Bickford J.H., An Introduction to the Design and Behavior of Bolted Joints, Second Edition, Marcel Dekker, NY, 1990.
[16] Brown M., Durbin B., Guideline for Bolted Joint Design and Analysis: Version 1.0. Sandia Report, SAND2008-0371, Sandia National Laboratories for United States Dept. of Energy, 2013, p.12.

[17] Konter A., How to undertake a Contact and Friction Analysis, NAFEMS, Glasgow, 2000.
[18] Feng Q., Prinja N.K., Benchmark tests for finite element modelling of Contact, Gapping and Sliding, NAFEMS Report R0081, Glasgow, 2001.
[19] Gere J.M., Timoshenko S., Mechanics of Materials, Chapman & Hall, Third SI Edition, Boston, 1991, p.636.